Journal of Solid State Chemistry 182 (2009) 3262–3268

Contents lists available at ScienceDirect

Journal of Solid State Chemistry

journal homepage: www.elsevier.com/locate/jssc

Crystal structure and magnetic properties of Li,Cr-containing molybdates $Li_3Cr(MoO_4)_3$, $LiCr(MoO_4)_2$ and $Li_{1.8}Cr_{1.2}(MoO_4)_3$

A. Sarapulova [a,c], D. Mikhailova [a,b,*], A. Senyshyn [b], H. Ehrenberg [a,b]

[a] Institute for Complex Materials, IFW Dresden, Helmholtzstr. 20, D-01069 Dresden, Germany
[b] Institute for Materials Science, Darmstadt University for Technology, Petersenstr. 23, D-64287, Darmstadt, Germany
[c] Baikal Institute of Nature Management SD RAS, Ulan-Ude, Russia

ARTICLE INFO

Article history:
Received 28 June 2009
Received in revised form
9 September 2009
Accepted 11 September 2009
Available online 19 September 2009

PACS:
61.66.Fn

Keywords:
CrLi-molybdates
Mixed occupancy of cations
Antiferromagnetic structure
Superexchange couplings

ABSTRACT

Single crystals of $LiCr(MoO_4)_2$, $Li_3Cr(MoO_4)_3$ and $Li_{1.8}Cr_{1.2}(MoO_4)_3$ were grown by a flux method during the phase study of the Li_2MoO_4–$Cr_2(MoO_4)_3$ system at 1023 K. $LiCr(MoO_4)_2$ and $Li_3Cr(MoO_4)_3$ single phases were synthesized by solid-state reactions. $Li_3Cr(MoO_4)_3$ adopts the same structure type as $Li_3In(MoO_4)_3$ despite the difference in ionic radii of Cr^{3+} and In^{3+} for octahedral coordination. $Li_3Cr(MoO_4)_3$ is paramagnetic down to 7 K and shows a weak ferromagnetic component below this temperature. $LiCr(MoO_4)_2$ is isostructural with $LiAl(MoO_4)_2$ and orders antiferromagnetically below 20 K. The magnetic structure of $LiCr(MoO_4)_2$ was determined from low-temperature neutron diffraction and is based on the propagation vektor $\vec{k}=(\frac{1}{2},\frac{1}{2},0)$. The ordered magnetic moments were refined to $2.3(1)\,\mu_B$ per Cr-ion with an easy axis close to the $[1\,1\,\bar{1}]$ direction. A magnetic moment of $4.37(3)\,\mu_B$ per Cr-ion was calculated from the Curie constant for the paramagnetic region.

The crystal structures of the hitherto unknown $Li_{1.8}Cr_{1.2}(MoO_4)_3$ and $LiCr(MoO_4)_2$ are compared and reveal a high degree of similarity: In both structures MoO_4-tetrahedra are isolated from each other and connected with CrO_6 and LiO_5 via corners. In both modifications there are Cr_2O_{10} fragments of edge-sharing CrO_6-octahedra.

1. Introduction

Li-containing molybdates with A^{3+} (A=Al, Ga, In, Sc, Cr, Fe, Bi or rare earth elements) crystallize mainly in two compositions, $LiA(MoO_4)_2$ (Li/A=1:1) and $Li_3A(MoO_4)_3$ (Li/A=3:1). They belong to several structure types [1] with different connectivity schemes of $[MoO_4]$-tetrahedra or $[MoO_6]$-octahedra, depending on the A/Mo-ratio and the size of the A-cation. For Li/A=1:1 and A-cations with ionic radii about 1 Å (for octahedral oxygen coordination) such as Bi^{3+} or rare-earth elements sheelite-like structures are formed. In this structure, Li and A cations are statistically distributed over Ca positions of scheelite $CaWO_4$. For $LiLa(MoO_4)_2$, a low-temperature orthorhombic α-polymorph with MoO_4-tetrahedra, LiO_5- and LaO_9-polyhedra is also known [1]. LaO_9-polyhedra form edge-shared dimers, which are connected with each other via MoO_4-tetrahedra through corners and edges. For smaller A^{3+}-cations with ionic radii about 0.5–0.6 Å such as Al, Ga, Cr or Fe, a structure containing isolated layers of LiO_5 trigonal bipyramids and AO_6-octahedra, separated by layers of isolated MoO_4-tetrahedra, is formed; this is the $LiAl(MoO_4)_2$ structure type [2,3]. For medium-sized cations In^{3+} (0.80 Å) and Sc^{3+} (0.75 Å) two polymorphic modifications with Li/A=1:1 exist depending on the synthesis temperature or pressure: the low-temperature form of $LiIn(MoO_4)_2$ adopts a wolframite-like structure with distorted MoO_6-octahedra [4] as well as the high-pressure modification of $LiSc(MoO_4)_2$ [5]. The high-temperature modification of $LiIn(MoO_4)_2$ [6] crystallizes in the $LiAl(MoO_4)_2$ structure type, whereas the structure of the normal pressure modification of $LiSc(MoO_4)_2$ is not yet determined [7].

Compositions $Li_3A(MoO_4)_3$ are known for A=Al, Ga, In, Sc, Fe and Cr [1,2,7–11]: they seem to adopt a common structure type, representing a pseudohexagonal framework of two types of edge- and corner-sharing $(Li,A)O_6$-octahedra and chains of LiO_6 trigonal prisms.

Two phases, $Li_3Cr(MoO_4)_3$ and $LiCr(MoO_4)_2$ with Cr^{3+}, are known in the system Li_2MoO_4–$Cr_2(MoO_4)_3$. $Li_3Cr(MoO_4)_3$ can be synthesized from Li- and Cr-molybdates at 623 K in air and melts incongruently at 1013 K [10,11]. Based on the similarity of X-ray diffraction patterns it was assumed that $Li_3Cr(MoO_4)_3$ adopts the same structure type as $Li_3In(MoO_4)_3$ [7]. Some Li-ions are situated in the trigonal prismatic channels along the *a*-axis and provide ionic conductivity comparable to the conductivity of well known one-dimensional lithium ion conductors such as $LiAlSiO_4$ [12]. $LiCr(MoO_4)_2$ forms at 723 K in air and is thermally more stable: it melts with decomposition at 1093 K [1]. $LiCr(MoO_4)_2$ is

* Corresponding author at: Institute for Materials Science, Darmstadt University for Technology, Petersenstr. 23, D-64287, Darmstadt, Germany.
E-mail address: d.mikhailova@ifw-dresden.de (D. Mikhailova).

0022-4596/$ - see front matter © 2009 Elsevier Inc. All rights reserved.
doi:10.1016/j.jssc.2009.09.012

isostructural with $LiAl(MoO_4)_2$ [2], but no detailed structural information is presented in the literature. No structural phase transitions are reported for Li,Cr-molybdates.

$LiCr(MoO_4)_2$ orders antiferromagnetically at 20 K and obeys a Curie–Weiss law in the temperature range of 30–300 K with a paramagnetic moment of 3.79 μ_B [13]. Magnetic properties of $Li_3Cr(MoO_4)_3$ were not yet investigated. A crystal structure like the one of $Li_3Cr(MoO_4)_3$ was proposed for the Cr-containing double chromate–molybdate $3Li_2CrO_4\cdots Cr_2(MoO_4)_3$ [10] with Cr^{+3} and Cr^{+6} due to the similar diffraction patterns of these compounds.

In this work we describe the crystal structural features of $Li_3Cr(MoO_4)_3$, $LiCr(MoO_4)_2$ and $Li_{1.8}Cr_{1.2}(MoO_4)_3$, based on X-ray single crystal data, together with the magnetic properties of the first two compounds.

2. Experimental

Syntheses of $LiCr(MoO_4)_2$ and $Li_3Cr(MoO_4)_3$ powders at ambient pressure were performed from Li_2MoO_4 (Alfa Aesar, 99%), MoO_3 (Alfa Aesar, 99.95%) and $Cr(NO_3)_3\cdot 9H_2O$ (Alfa Aesar, 99.99%) in air in porcelain crucibles. Mixtures with a total mass of 2–3 g were weighed with an accuracy of 0.0005 g, ground together in an agate mortar and placed within a crucible into a muffel furnace. The synthesis temperature was 873 K, the reaction time 50–80 h. Single crystals of $LiCr(MoO_4)_2$, $Li_3Cr(MoO_4)_3$ and $Li_{1.8}Cr_{1.2}(MoO_4)_3$ were grown by the flux method during the phase study of the Li_2MoO_4–$Cr_2(MoO_4)_3$ system at 1023 K in air, too. High-pressure experiments on $Li_3Cr(MoO_4)_3$ were performed at 773 K and 9 GPa in an octahedral multianvil press described elsewhere [14]. As starting material $Li_3Cr(MoO_4)_3$ obtained in air was used. Pressure transmission and redistributon is realized by MgO-octahedra, the reaction temperature was adjusted by resistance heating using graphite tubes. Hexagonal boron nitride was used as crucible material, no reaction of the crucible with the sample was observed.

Phase analysis and determination of cell parameters at room temperature and high-temperature structure investigations (up to 973 K) of $LiCr(MoO_4)_2$ and $Li_3Cr(MoO_4)_3$ were carried out using X-ray powder diffraction (XPD) with a STOE STADI P diffractometer (Mo-$K\alpha_1$-radiation, λ=0.7093 Å) in transmission mode.

Crystal structures of $LiCr(MoO_4)_2$, $Li_{1.8}Cr_{1.2}(MoO_4)_3$ and $Li_3Cr(MoO_4)_3$ were determined using single-crystal X-ray diffraction using the Xcalibur system from Oxford Diffraction. The software packages SHELXS [15] and SHELXL [16] were used for structure solution and refinement as included in X-STEP32 [17]. A combined empirical absorption correction with frame scaling was applied, using the SCALE3 ABSPACK command in CrysalisRed [18].

Magnetic structure of $LiCr(MoO_4)$ was determined from neutron powder diffraction data, SPODI, FRM II (Munich) [19]. Two data sets, one at 50 K above the magnetic ordering temperature and one at 3 K below, were measured with neutrons of 2.5360(1) Å wavelength.

All diffraction patterns were analyzed by full-profile Rietveld refinements, using the software package WinPLOTR [20]. The structure model was refined with an isotropic approximation for the thermal displacement parameters of all atoms, which were constrained into four groups: one value for all oxygen atoms, one for Mo, one for Cr and one for Li.

Magnetic properties of $LiCr(MoO_4)_2$ and $Li_3Cr(MoO_4)_3$ have been studied with a superconducting quantum interference device (SQUID) from Quantum Design. Measurements were performed in field-cooled and zero-field cooled mode in the temperature range from 1.8 to 350 K and with external magnetic field strengths of 500 G.

Quantitative determination of Li, Cr and Mo contents in $LiCr(MoO_4)_2$ and $Li_3Cr(MoO_4)_3$ was carried out by ICP-OES method (IRIS Intrepid II XUV, Thermo Fisher) using a mixture of HCl (37%, p.a. Fa. Merck), HNO_3 (65%, p.a. Fa. Merck) and $KClO_3$ (99.0%, Fa. Merck) for dissolving the samples. Three independent measurements on weighed portions of about 30 mg were performed for each composition.

3. Results and discussion

3.1. Syntheses and phase characterizations

$LiCr(MoO_4)_2$ and $Li_3Cr(MoO_4)_3$ were obtained at 773 K and ambient pressure as single phases, their powder diffraction patterns are presented in Fig. 1. All reflections for $LiCr(MoO_4)_2$ were explained based on a triclinic unit cell with the lattice parameters a=6.7074(1) Å, b=7.1586(1) Å, c=7.2353(1) Å, α=91.109(1)°, β=110.415(1) Å, γ=105.478(1)° and for $Li_3Cr(MoO_4)_3$ on an orthorhombic unit cell with the lattice parameters a=5.0737(1) Å, b=10.4031(2) Å and c=17.4502(3) Å. According to the results of the chemical analysis, normalized on the Li-content, the compounds are stoichiometric: $Li_{1.00}Cr_{1.04(3)}Mo_{2.04(2)}O_8$ and $Li_{3.00}Cr_{1.02(2)}Mo_{3.00(3)}O_{12}$. No phase transitions were registered for $LiCr(MoO_4)_2$

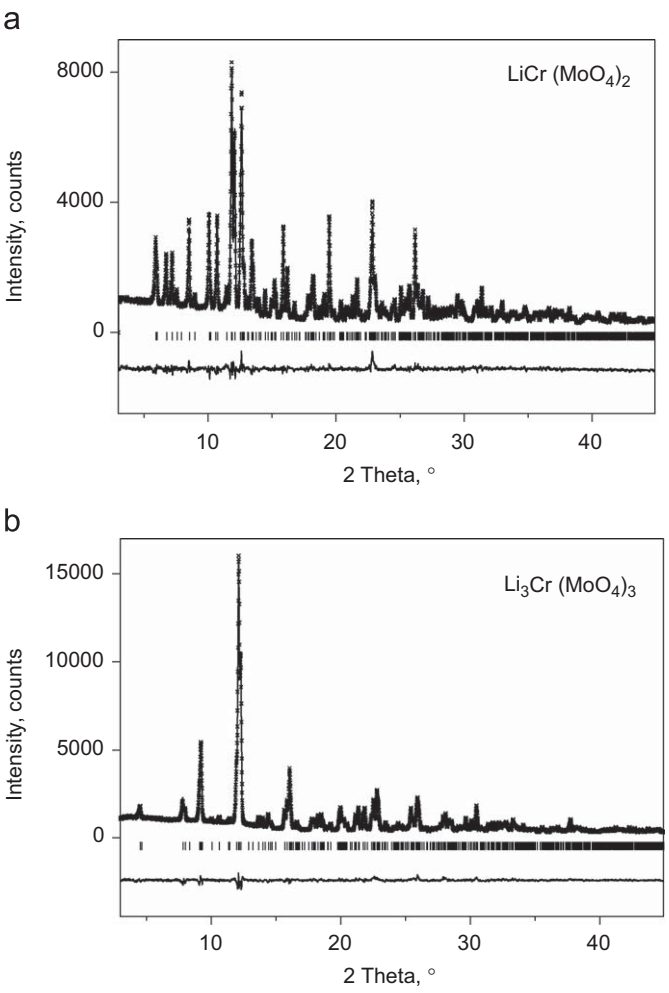

Fig. 1. (a) Measured and calculated powder diffraction pattern for $LiCr(MoO_4)_2$ together with the difference curve (Mo-$K\alpha_1$ radiation). (b) Measured and calculated powder diffraction pattern for $Li_3Cr(MoO_4)_3$ together with the difference curve (Mo-$K\alpha_1$ radiation).

and $Li_3Cr(MoO_4)_3$ up to 973 K by high-temperature X-ray diffraction. High-pressure experiments at 873 K on $Li_3Cr(MoO_4)_3$ have shown the stability of this phase: it does not transform into a metastable high-pressure phase. $LiCr(MoO_4)_2$ and $Li_3Cr(MoO_4)_3$ decompose partially in the solid state before melting: all attempts to anneal these phases at temperatures 30–0 K below their melting point led to the formation of multiphase samples containing Cr_2O_3 and Li-polymolybdates.

$Li_{1.8}Cr_{1.2}(MoO_4)_3$ crystals were found in a multiphase sample, obtained from a mixture containing Li_2MoO_4, Cr_2O_3 and MoO_3 in the molar ratio of 7:3:9 after heating to 1023 K in air. The conditions for the formation of this phase are still unclear; it was impossible to obtain this modification in pure form.

3.2. Crystal structures of $LiCr(MoO_4)_2$, $Li_3Cr(MoO_4)_3$ and $Li_{1.8}Cr_{1.2}(MoO_4)_3$

According to the X-ray single crystal experiments, $LiCr(MoO_4)_2$ crystallizes in a triclinic unit cell similar to $LiAl(MoO_4)_2$ [2] (Table 1). All atoms occupy general positions (Table 2), there is no mixed occupancy between Li and Cr ions. Each CrO_6-octahedron shares edges with other CrO_6-octahedra and LiO_5-pyramids, so that a structural fragment consisting of a $(LiO_5)(CrO_6)(CrO_6)(LiO_5)$-sequence can be isolated (Fig. 2). There are no channels in the structure: Li-atoms are placed in distorted tetragonal pyramids and undergo strong covalent binding with O-atoms with an average Li–O distance of about 2.124 Å, corresponding to the sum of ionic radii of Li^+ for coordination number 5 and O^{2-} [21]. No high ionic conductivity of Li is expected for this structure, even at elevated temperatures.

$Li_{1.8}Cr_{1.2}(MoO_4)_3$ crystallizes also with triclinic symmetry (Table 1). There are three different sites for Li and Cr atoms in the structure, two of them are statistically occupied by Li and Cr, forming $(Li,Cr)O_6$-octahedra, and one site is completely occupied by Li atoms and surrounded by distorted tetragonal pyramids of oxygen atoms (Fig. 3). The determined composition corresponds to the minimum of the R_1-factors. The formal average oxidation state of Cr in $Li_{1.8}Cr_{1.2}(MoO_4)_3$ is +3.5 for an assignment of Mo(VI) (Table 3).

Some similarities exist between the crystal structures of $LiCr(MoO_4)_2$ and $Li_{1.8}Cr_{1.2}(MoO_4)_3$: MoO_4-tetrahedra are isolated from each other and connected with CrO_6 and LiO_5 via corners. In both phases there are Cr_2O_{10} fragments of edge-sharing CrO_6-octahedra. The topology of the MoO_4-tetrahedra network is also resembled, see Fig. 4.

Note that the structure of $Li_{1.8}Cr_{1.2}(MoO_4)_3$ (3.950 g/cm^3) is less dense than the one of $LiCr(MoO_4)_2$ (4.060 g/cm^3) due to the mixed occupancy of Li^+ (0.76 Å) and Cr^{3+} (0.62 Å)/Cr^{4+} (0.55 Å) atoms.

$Li_3Cr(MoO_4)_3$ is isostructural to $Li_3M(MoO_4)_3$ with M=Sc [9] or Fe [22]. This structure type was first described for the Na,Co-containing molybdate with $NaCo_{2.31}(MoO_4)_3$ stoichiometry [25]. From a structural point of view the composition $Li_3Cr(MoO_4)_3$ is

Table 1
Details of X-ray single-crystal data collection and structure refinement of $LiCr(MoO_4)_2$, $Li_3Cr(MoO_4)_3$ and $Li_{1.8}Cr_{1.2}(MoO_4)_3$.

Crystal data			
Chemical formula	$LiCr(MoO_4)_2$	$Li_3Cr(MoO_4)_3$	$Li_{1.8}Cr_{1.2}(MoO_4)_3$
Formula weight	378.82	552.64	259.79
Crystal system	Triclinic	Orthorhombic	Triclinic
Space group	$P-1$	*Pnma*	P−1
Unit cell dimensions, (Å)°	a=6.703(5) Å, b=7.148(7) Å, c=7.224(5) Å, α=91.09(7)°, β=110.48(7)°, γ=105.62(7)°	a=5.0770(8) Å, b=10.438(2) Å, c=17.483(2) Å	a=6.7191(5) Å, b=6.8268(6) Å, c=11.3467(11) Å, α=77.648(8)°, β=85.610(7)°, γ=77.782(7)°
Cell volume (Å^3)	309.8(4)	926.5(3)	496.64(7)
Z	2	4	2
Calculated density (g/cm^3)	4.060	3.962	3.950
Radiation type	Mo-Kα, λ=0.71073 Å		
Temperature (K)	299(2)	299(2)	298(2)
Crystal form, colour	prismatic, black	needle-shaped, red	prismatic, brown
Crystal size (mm^3)	0.060 × 0.025 × 0.025	0.50 × 0.05 × 0.05	0.10 × 0.04 × 0.03
Data collection			
Diffractometer	Oxford Diffraction Xcalibur; single-crystal X-ray diffractometer with sapphire CCD detector		
Data collection method	Rotation method data acquisition using ω and φ scans(s)		
Absorption coefficient (mm^{-1})	5.708	5.171	5.860
F(000)	350	1020	546
Theta range for data collection	2.98–27.97°	3.90–26.36°	3.10–27.87°
Range of h, k, l	$-8 \le h \le 8$, $-6 \le k \le 9$, $-8 \le l \le 9$	$-6 \le h \le 4$, $-9 \le k \le 13$, $-21 \le l \le 17$	$-8 \le h \le 8$, $-8 \le k \le 8$, $-14 \le l \le 14$
Reflections collected/unique	1662/1129	2480/963	4491/2098
Refinement method	Full-matrix least-squares on F^2		
Data/restraints/parameters	1129/0/109	963/4/98	2098/0/165
Goodness-of-fit on F^2	1.094	1.156	1.016
Final R indices [I > 2sigma(I)]	R_1=0.0251, wR_2=0.0614	R_1=0.0403, wR_2=0.1094	R_1=0.0245, wR_2=0.0664
R indices (all data)	R_1=0.0407, wR_2=0.0637	R_1=0.0438, wR_2=0.1148	R_1=0.0335, wR_2=0.0683
Largest diff. peak and hole	0.812, −0.832 e/Å^3	1.860, −1.516 e/Å^3	2.016, −0.865 e/Å^3

Table 2
Positional parameters and equivalent isotropic displacement parameters for $LiCr(MoO_4)_2$, $Li_3Cr(MoO_4)_3$ and $Li_{1.8}Cr_{1.2}(MoO_4)_3$.

Atom	Site	x	y	z	U_{iso} (Å^2)	Occup.
$LiCr(MoO_4)_2$						
Mo(1)	2*i*	0.32397(9)	0.46926(7)	0.21820(9)	0.0081(2)	1
Mo(2)	2*i*	−0.16939(9)	0.07426(7)	0.28816(9)	0.0107(2)	1
Cr	2*i*	−0.0906(2)	0.6001(1)	0.3237(2)	0.0099(2)	1
Li	2*i*	−0.7308(15)	−0.0501(12)	0.2612(17)	0.008(2)	1
O(1)	2*i*	−0.0783(7)	0.3401(6)	0.3873(7)	0.0092(9)	1
O(2)	2*i*	−0.2530(8)	0.0729(6)	0.0386(7)	0.020(1)	1
O(3)	2*i*	0.6177(7)	0.5544(6)	0.3491(7)	0.011(1)	1
O(4)	2*i*	0.2582(7)	0.4651(6)	−0.0392(7)	0.016(1)	1
O(5)	2i	−0.0211(7)	−0.1161(6)	0.3440(7)	0.013(1)	1
O(6)	2*i*	0.1901(7)	0.6332(6)	0.2804(7)	0.010(1)	1
O(7)	2*i*	0.2197(8)	0.2306(6)	0.2571(7)	0.017(1)	1
O(8)	2*i*	−0.4047(8)	−0.0166(6)	0.3372(8)	0.019(1)	1
$Li_3Cr(MoO_4)_3$						
Mo(1)	8*d*	0.2776(1)	0.5252(1)	0.1565(1)	0.0108(3)	1
Mo(2)	4*c*	0.7807(1)	0.25	0.0576(1)	0.0097(3)	1
Cr(1)	4*c*	0.1068(6)	0.25	0.2501(2)	0.011(1)	0.383(1)
Li(1)	4*c*	0.1068(6)	0.25	0.2501(2)	0.011(1)	0.617(1)
Cr(2)	8*d*	0.7562(5)	0.5695(3)	0.0250(2)	0.0162(7)	0.308(1)
Li(2)	8*d*	0.7562(5)	0.5695(3)	0.0250(2)	0.0162(7)	0.692(1)
Li(3)	4*c*	0.2440(30)	0.75	0.3031(9)	0.015(3)	1
O(1)	4*c*	0.8599(14)	0.25	0.1570(3)	0.018(1)	1
O(2)	4*c*	0.0565(13)	0.25	−0.0056(3)	0.018(1)	1
O(3)	8*d*	0.5806(8)	0.1156(4)	0.0370(2)	0.0165(9)	1
O(4)	8*d*	0.0792(9)	0.4873(4)	0.0748(2)	0.0166(9)	1
O(5)	8*d*	0.0807(9)	0.6229(4)	0.2132(2)	0.021(1)	1
O(6)	8*d*	0.3559(9)	0.3802(4)	0.2056(2)	0.0158(9)	1
O(7)	8*d*	0.5596(9)	0.6116(4)	0.1262(2)	0.0173(9)	1
$Li_{1.8}Cr_{1.2}(MoO_4)_3$						
Mo(1)	2*i*	−0.24684(6)	0.09542(6)	−0.15097(3)	0.0052(1)	1
Mo(2)	2*i*	−0.29701(6)	0.28572(6)	0.19018(4)	0.0073(1)	1
Mo(3)	2*i*	0.24592(6)	0.30289(6)	−0.45005(3)	0.0058(1)	1
Cr(1)	2*i*	−0.1969(2)	0.1599(2)	−0.4784(1)	0.0046(4)	0.531(3)
Li(1)	2*i*	−0.1969(2)	0.1599(2)	−0.4784(1)	0.0046(4)	0.469
Cr(2)	2*i*	−0.1940(2)	−0.2323(2)	0.1258(1)	0.0041(4)	0.680(3)
Li(2)	2*i*	−0.1940(2)	−0.2323(2)	0.1258(1)	0.0041(4)	0.320
Li(3)	2*i*	−0.176(1)	−0.438(1)	−0.0876(7)	0.013(2)	1
O(1)	2*i*	−0.2010(5)	−0.1491(5)	−0.0515(3)	0.0077(7)	1
O(2)	2*i*	−0.1639(5)	0.4809(5)	0.1062(3)	0.0091(7)	1
O(3)	2*i*	−0.1091(5)	0.2685(5)	−0.1143(3)	0.0076(7)	1
O(4)	2*i*	−0.5076(5)	0.2004(5)	−0.1417(3)	0.0113(7)	1
O(5)	2*i*	−0.2486(5)	0.2450(5)	0.3428(3)	0.0135(8)	1
O(6)	2*i*	−0.1788(5)	0.0586(5)	−0.2966(3)	0.0108(7)	1
O(7)	2*i*	0.5015(5)	0.1904(5)	−0.4536(3)	0.0137(8)	1
O(8)	2*i*	0.1126(5)	0.1366(5)	−0.5034(3)	0.0089(7)	1
O(9)	2*i*	0.1741(5)	0.3205(5)	−0.3005(3)	0.0113(7)	1
O(10)	2*i*	0.2061(5)	0.5506(5)	−0.5407(3)	0.0110(7)	1
O(11)	2*i*	−0.5548(5)	0.3595(6)	0.1696(3)	0.0180(8)	1
O(12)	2*i*	−0.2112(5)	0.0536(5)	0.1389(3)	0.0109(7)	1

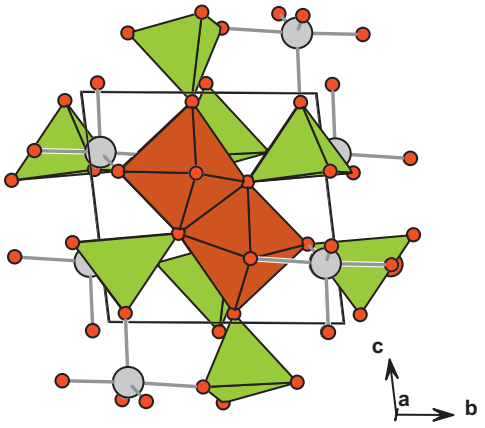

Fig. 2. Projection of the crystal structure of $LiCr(MoO_4)_2$ along the *a*-axis: Cr atoms occupy octahedra of oxygen atoms (brown), green—MoO_4-tetrahedra, large light spheres—Li atoms. For interpretation of the references to colour in this figure legend, the reader is referred to the web version of this article.

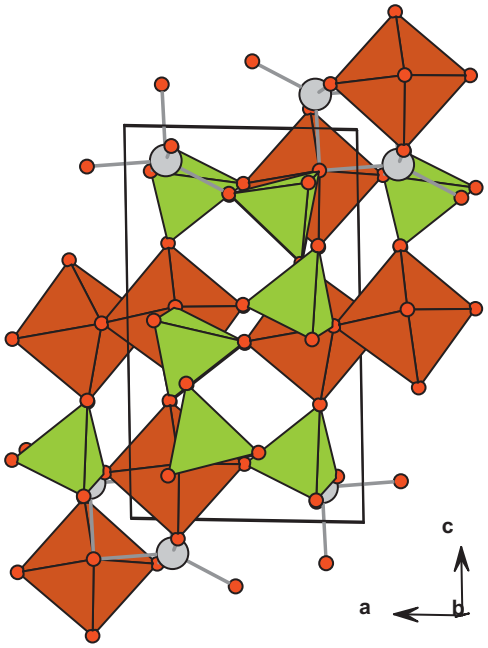

Fig. 3. Projection of the crystal structure of $Li_{1.8}Cr_{1.2}(MoO_4)_3$ along the *b*-axis. Cr and Li atoms occupy oxygen octahedra (brown), green—MoO_4-tetrahedra, large light spheres—Li atoms. For interpretation of the references to colour in this figure legend, the reader is referred to the web version of this article.

better described as $AB_2C(MoO_4)_3$ with A=$Cr_{0.383(1)}Li_{0.617}$, B=$Cr_{0.308(1)}Li_{0.692}$ and C=Li. In the structure, there are two types of (Li,Cr)-octahedra: infinite chains of face-sharing AO_6 along [1 0 0] and networks of corner and edge-sharing BO_6 parallel to (0 0 1). The isolated MoO_4-tetrahedra connect networks and chains via corner into a pseudohexagonal framework with channels parallel to [1 0 0], which are occupied only by Li-atoms. The average Li–O distances are of 2.031(3) and 2.084(5) Å for mixed (Li,Cr)O_6-octahedra and 2.17(1) Å for Li-atoms in the channels (Fig. 5) for LiO_6 trigonal prisms. The Li–O bonds in channels have a more ionic character than the Li–O bond in $LiCr(MoO_4)_2$. Different synthesis temperatures (up to 873 K) do not influence significantly the degree of the cation disorder (Li,Cr) on the 4*c* and 8*d* sites.

Table 3
Selected average interatomic distances (Å) for $LiCr(MoO_4)_2$, $Li_3Cr(MoO_4)_3$ and $Li_{1.8}Cr_{1.2}(MoO_4)_3$.

	$Li_3Cr(MoO_4)_3$	$LiCr(MoO_4)_2$	$Li_{1.8}Cr_{1.2}(MoO_4)_3$
Mo(1)–O	1.772(4)	1.766(5)	1.763(3)
Mo(2)–O	1.777(5)	1.782(6)	1.762(3)
Mo(3)–O			1.761(3)
Cr(1)–O	2.031(6)	1.954(6)	2.028(4)
Cr(2)–O	2.084(5)		1.973(3)
Li(1)–O	2.031(6)	2.12(1)	2.028(4)
Li(2)–O	2.084(5)		1.973(3)
Li(3)–O	2.17(1)		2.103(9)

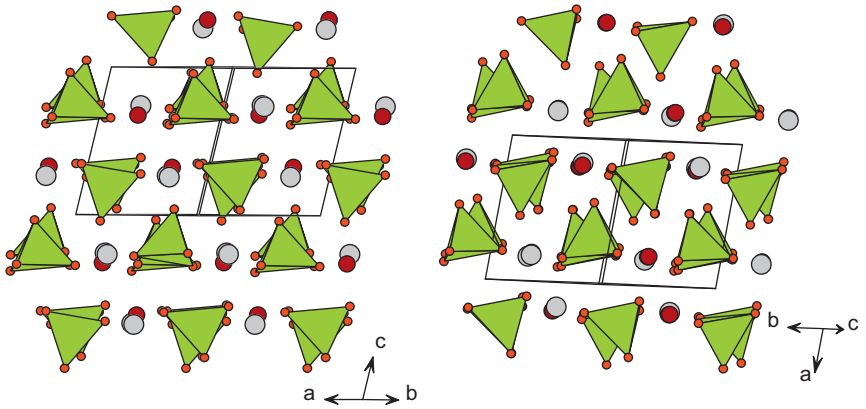

Fig. 4. Structural fragments of $LiCr(MoO_4)_2$ (left) and $Li_{1.8}Cr_{1.2}(MoO_4)_3$ (right). Brown spheres are Cr atoms for $LiCr(MoO_4)_2$ and Cr,Li atoms for $Li_{1.8}Cr_{1.2}(MoO_4)_3$. Light-grey spheres are Li atoms, MoO_4-tetrahedra are green. For interpretation of the references to colour in this figure legend, the reader is referred to the web version of this article.

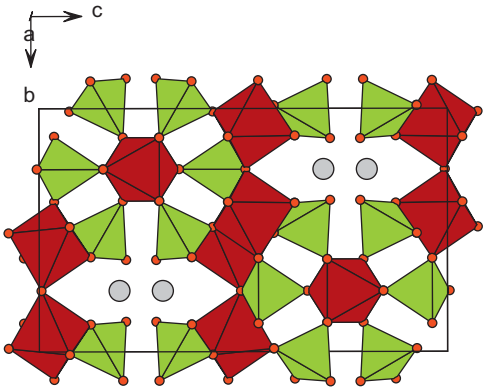

Fig. 5. Projection of the crystal structure of $Li_3Cr(MoO_4)_3$ on (1 0 0). Coordination polyhedra for Cr and partly for Li atoms are octahedra (brown), another part of Li atoms (grey spheres) is situated in channels with larger Li–O distances. For interpretation of the references to colour in this figure legend, the reader is referred to the web version of this article.

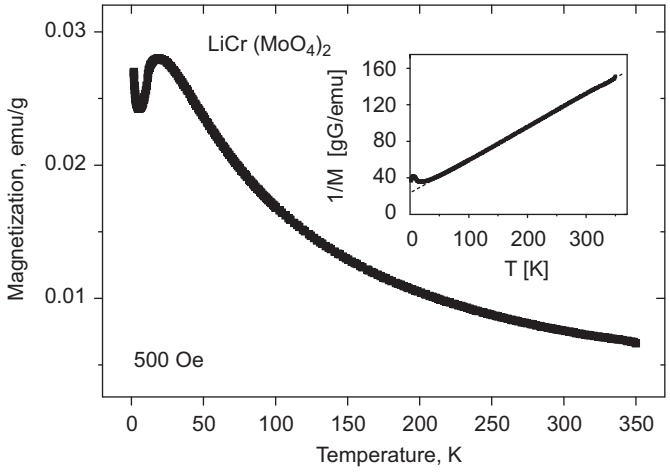

Fig. 6. Temperature dependence of magnetization for $LiCr(MoO_4)_2$.

3.3. Magnetic properties of $LiCr(MoO_4)_2$ and $Li_3Cr(MoO_4)_3$

The temperature dependence of magnetization of $LiCr(MoO_4)_2$ demonstrates a maximum at ca. 20 K in agreement with the literature [13] (Fig. 6). $Li_3Cr(MoO_4)_3$ is paramagnetic down to 7 K,

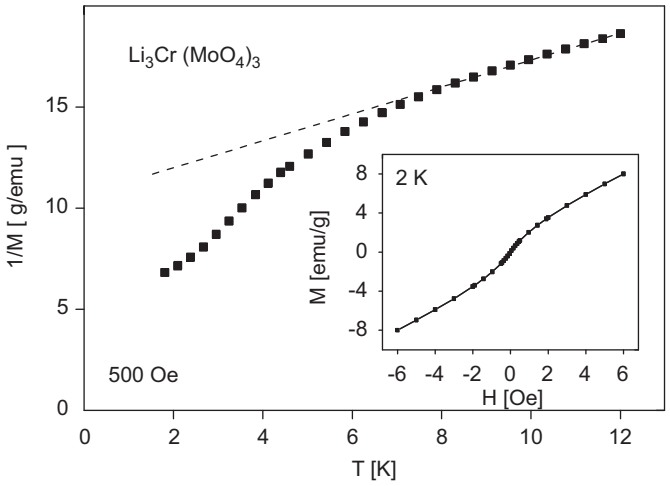

Fig. 7. Temperature and field dependence (inset) of magnetization for $Li_3Cr(MoO_4)_3$.

Table 4
Magnetic properties of $LiCr(MoO_4)_2$ and $Li_3Cr(MoO_4)_3$.

Compound	$T(\chi_{max})$ (K)	$\chi_0 \times 10^6$ (emu/gG)	Θ (K)	μ_{eff}(exp) (μ_B)	Temperature range for fit (K)
$LiCr(MoO_4)_2$	19(1)	−1.7(3)	−79(2)	4.37(3)	50–300
$Li_3Cr(MoO_4)_3$	–	−0.7(1)	−18.5(2)	3.91(1)	25–350

The standard deviations in brackets are determined as the limits, for which an up to 10% higher residual is obtained in the least-square fit than for the optimum fit for Eq. (1).

below this temperature a weak ferromagnetic component appears (Fig. 7). A weak ferromagnetic component was also found for orthorhombic $Li_3Fe(MoO_4)_3$ [23] with the lyonsite-type structure below 10 K. This is rather surprising in the light of the diluted character of the Cr (or Fe) distribution in the structure. The characteristic magnetic parameters of these compounds in the paramagnetic region are obtained from fitting Eq. (1) to the observed data and presented in Table 4.

$$M(T) = \frac{C}{T-\theta} + M_0 \quad (1)$$

3.4. Magnetic structure of $LiCr(MoO_4)_2$

The magnetic structure of $LiCr(MoO_4)_2$ was determined based on neutron powder diffraction data collected at 3 K (Fig. 8). All

magnetic reflections can be indexed, based on the propagation vector $k=(\frac{1}{2}, \frac{1}{2}, 0)$ and confirm the antiferromagnetic ordering at low temperature, indicated by the temperature dependence of magnetization. The observed magnetic Bragg intensities are in agreement with the collinear antiferromagnetic model shown in Fig. 9. The projections of the Cr magnetic moments on the *x*-, *y*-, *z*-axis are $\mu_x=1.2(2)\,\mu_B$, $\mu_y=1.2(2)\,\mu_B$, $\mu_z=-1.4(2)\,\mu_B$ with a total moment of $2.3(1)\,\mu_B$. This antiferromagnetic arrangement is discussed in the light of the underlying superexchange interactions. Only one superexchange coupling J_0 exists with a Cr–O–Cr angle of 99.7°. The corresponding spin pairs are always antiparallel to each other as expected from the Kanamori rules for Cr^{3+} in the 90° superexchange case. The supersuperexchange coupling paths Cr–O–O–Cr with both oxygens from one coordination polyhedra of Li or Mo are listed in Table 5. Larger Cr–Cr distances correspond to larger Cr–O–O and O–O–Cr angles and, therefore, dominant antiferromagnetic couplings are expected for those supersuperexchange couplings. Indeed, the two interactions J_1 and J_2 with angles close to 180° result in antiferromagnetic couplings and explain the doubling of the magnetic unit cell along the *a*- and *b*-axis with respect to the crystallographic one. The three couplings J_0, J_1 and J_2 result in antiferromagnetic layers of pairs of CrO_6-octahedra parallel to the *ab*-planes, but do not allow any conclusion about the sequence along the *c*-axis. All supersuperexchange couplings, which bridge the above mentioned layers to a three-dimensional magnetic structure, correspond to parallel alignments of the magnetic moments, see column 2 in Table 5, and the Cr–Cr distances are rather short, resulting from Cr–O–O or O–O–Cr angles closer to 90° than to 180°. It seems that supersuperexchange couplings Cr^{3+}–O–O–Cr^{3+} change sign from antiferromagnetic to ferromagnetic with decreasing angles along the coupling paths deviating more and more from the collinear 180° angles and approaching 90°. Such a tendency was already previously observed in the similar compound $NaCr(WO_4)_2$, but with a different crystal structure type [24]. Such ferromagnetic supersuperexchange couplings would complete the necessary set of magnetic interactions to explain the observed three-dimensional magnetic structure. Alternative explanations, based on long-range magnetic exchange or the magnetic dipole–dipole interaction, cannot be excluded, but appear less plausible in the light of the rather high ordering temperature. The broad maximum in the temperature dependence of magnetization might reflect the dominant couplings within two dimensions and a weaker coupling between the layers.

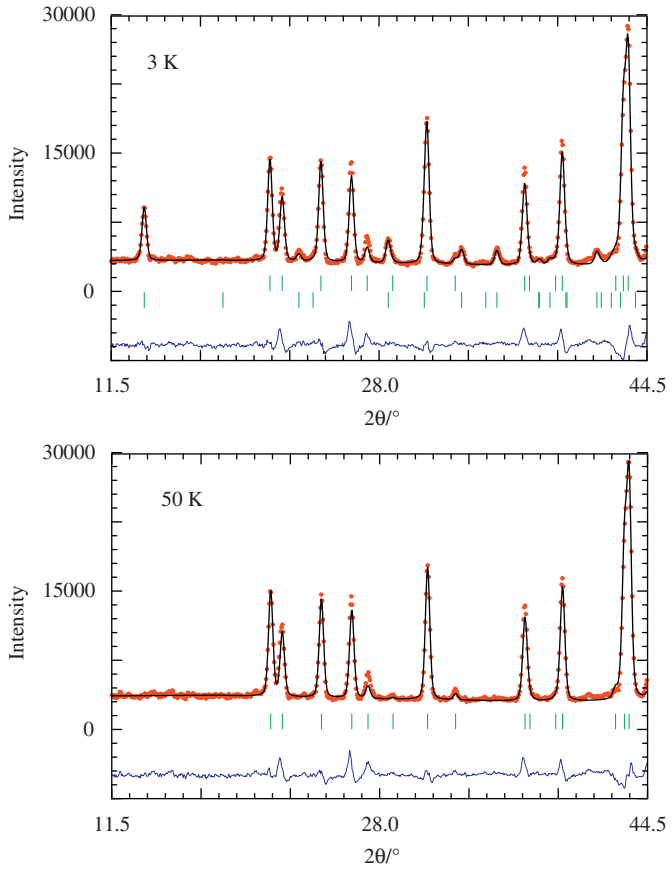

Fig. 8. Neutron diffraction patterns of $LiCr(MoO_4)_2$ at 3 and 50 K together with calculated intensities and the difference curve (at the bottom). The upper line of reflection marks at 3 K corresponds to the crystal structure, the lower line to the magnetic Bragg peaks.

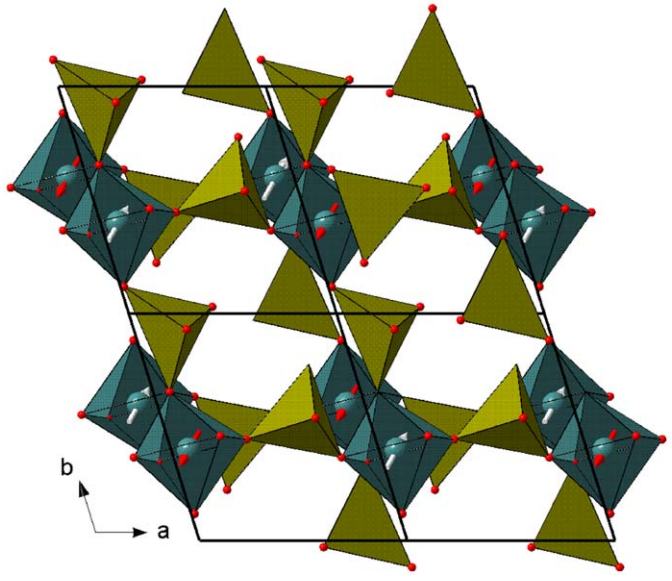

Fig. 9. Magnetic structure of $LiCr(MoO_4)_2$. The orientation of the magnetic moments of Cr^{3+} is shown by arrows.

Table 5
Geometry of the magnetic superexchange coupling path J_0 and the super-superexchange couplings via two oxygens of one coordination polyhedron.

J	F/AF	d_1 (Å)	α (deg)	d_2 (Å)	(x,y,z)	d(Cr–Cr) (Å)
J_0	↑↓	1.939	99.7	1.969	$(-x,1-y,1-z)$	2.987

J	F/AF	d_1 (Å)	α_1 (°)	d(O–O) (Å)	α_2 (°)	d_2 (Å)	(x,y,z)	d(Cr–Cr) (Å)
J_1	↑↓	1.946	160.1	3.405	159.3	1.939	$(x,y\pm1,z)$	7.148
J_2	↑↓	1.967	153.7	2.943	154.1	1.968	$(x\pm1,y,z)$	6.703
J_3	↑↑	1.969	95.9	3.405	160.1	1.946	$(-x,2-y,1-z)$	5.847
J_4	↑↑	1.941	162.7	2.908	111.3	1.968	$(-x-1,1-y,-z)$	5.621
J_5	↑↑	1.967	128.6	2.812	134.7	1.941	$(-x,1-y,-z)$	5.482

Acknowledgement

The authors are indebted to S. Leipe (Max-Planck Institute for Chemical Physics of Solids, Dresden, Germany) for performing the HPHT experiments on a multianvil press, and to A. Voss (Institute for Complex Materials, IFW Dresden, Germany) for performing chemical analysis.

This work was supported by the *Sächsisches Ministerium für Wissenschaft und Kunst*. The neutron powder diffractometer SPODI is funded by the *Bundesministerium für Bildung und Forschung* (03FU7DAR).

Appendix. Supporting Information

Supplementary data associated with this article can be found in the online version at doi:10.1016/j.jssc.2009.09.012.

References

[1] M.V. Mokhosoev, F.P. Alekseev, V.L. Butukhanov, Double Molybdates and Tungstates, Nauka, Novosibirsk, 1981.
[2] A. van der Lee, M. Beaurain, P. Armand, Acta Crystallogr. C 64 (2008) i1–i14.
[3] L.P. Solov'eva, S.V. Borisov, Kristallografiya 15 (1970) 577 (in Russian).
[4] M. Mączka, J. Hanuza, A. Pietraszko, J. Solid State Chem. 154 (2000) 498–506.
[5] Yu.A. Velikodnyi, V.K. Trunov, J. Inorg. Chem. 22 (1977) 1496–1498 (in Russian).
[6] Yu.A. Velikodnyi, V.A. Efremova, V.K. Trunov, Kristallografiya 25 (1980) 165–168 (in Russian).
[7] N.V. Porotnikov, V.V. Safonov, N.G. Chaban, K.I. Petrov, J. Inorg. Chem. 27 (1982) 1998–2002 (in Russian).
[8] P.V. Klevtsov, Kristallografiya 15 (1970) 797–802 (in Russian).
[9] Yu.A. Velikodnyi, V.K. Trunov, N.I. Markelova, J. Inorg. Chem. 15 (1970) 1170 (in Russian).
[10] V.L. Butukhanov, E.I. Get'man, M.V. Mokhosoev, J. Inorg. Chem. 21 (1976) 1409–1410 (in Russian).
[11] V.K. Trunov, Yu.A. Velikodnyi, Neorg. Mater. 8 (1972) 881–885.
[12] L. Sebastian, Y. Piffard, A.K. Shukla, F. Taulelle, J. Gopalakrishnan, J. Mater. Chem. 13 (2003) 1797–1802.
[13] J. Hanuza, M. Mączka, K. Hermanowicz, P.J. Dereń, W. Stręk, L. Folcik, H. Drulis, J. Solid State Chem. 148 (1999) 468–478.
[14] H. Huppertz, Z. Kristallogr. 219 (2004) 330.
[15] G.M. Sheldrick, Acta Crystallogr. A 46 (1990) 467–473.
[16] G.M. Sheldrick, SHELXL97, Program for the Refinement of Crystal Structures, University of Göttingen, Germany, 1997.
[17] Stoe & Cie, X-STEP32, 2000, Stoe & Cie GmbH, Darmstadt, Germany.
[18] CrysalisRed, CCD data reduction GUI, version 1.171.26, Oxford Diffraction Poland, 2005.
[19] M. Hoelzel, A. Senyshyn, R. Gilles, H. Boysen, H. Fuess, Neutron News 18 (4) (2007) 23.
[20] T. Roisnel, J. Rodriguez-Carvajal, Mater. Sci. Forum 378–381 (2001) 118–123.
[21] R.D. Shannon, Acta Crystallogr. A 32 (1976) 751–767.
[22] R.F. Klevtsova, S.A. Magarill, Kristallografiya 15 (1970) 710–715 (in Russian).
[23] M. Alvarez-Vega, U. Amador, M.E. Arroyo de Dompablo, J. Electrochem. Soc. 152 (2005) A1306–A1311.
[24] L. Nyam-Ochir, H. Ehrenberg, A. Buchsteiner, A. Senyshyn, H. Fuess, D. Sangaa, J. Magn. Magn. Mater. 320 (2008) 3251–3255.
[25] J.A. Ibers, G.W. Smith, Acta Crystallogr. 17 (1964) 190–197.